Strong re-entrant cellular structures with negative Poisson's ratio

Dong Li[a*], Jianhua Yin[b], Liang Dong[c], and Roderic S. Lakes[d]

[a] *College of Sciences, Northeastern University, Shenyang 110819, PR China*

[b] *Institute of Engineering Mechanics, China Earthquake Administration, Harbin, 150080, PR China*

[c] *Materials Science and Engineering, ,University of Virginia, Charlottesville, VA 22904, USA*

[d] *Department of Engineering Physics, University of Wisconsin, Madison, WI 53706-1687, USA*

*Corresponding author: Tel. +86 24 83678347; fax: +86 24 25962434; Email: lidong@mail.neu.edu.cn.

Preprint, Li, D., Yin, J., Dong, L. Lakes, R. S., "Strong re-entrant cellular structures with negative Poisson's ratio", *J. Materials Science*, 53, (5), 3493-3499 March (2018).

Dong Li: orcid.org/0000-0003-2546-8526
Jianhua Yin: orcd.org/0000-0001-8294-3798
Liang Dong: orcid.org/0000-0002-3646-8452
Roderic Lakes: orcid.org/0000-0001-9369-4184

Abstract: In this paper, two new 2D re-entrant topologies with negative Poisson's ratio are presented and their mechanical properties (Poisson's ratio and energy absorption capacity) are studied using finite element method (FEM) as a function of geometric parameters. The first topology (model 1) was constructed by adding two sinusoidal shaped ribs into the classical re-entrant topology, while the second topology (model 2) was made by introducing extra vertical ribs to reinforce the sinusoidal shaped ribs. Simulation results show that model 1 and model 2 topologies can reach a minimum value in Poisson's ratio of -1.12 and -0.58 with an appropriate geometric aspect ratio, respectively. The energy absorption capacities of model 1, model 2 and classical re-entrant model were studied at various compression velocities. Enhanced energy absorption capacities were observed in the two new re-entrant topologies compared with the classical re-entrant topology. Model 2 exhibited the highest energy absorption capacity and a highest plateau stress. The plateau stress of model 1 was about half that of model 2, and when the compression velocity is more than 20m/s, the plateau stress of model 1 became lower than that of the classical re-entrant model.

Keywords: Re-entrant; Cellular; Negative Poisson's ratio; Energy absorption; Property enhancement

1. Introduction

Cellular solids, including engineering honeycombs and foams, are widely used in many structural applications due to their unique properties, including high strength to weight ratio,

energy absorption, and diffusive transport properties. The mechanical properties of a cellular solid are determined by its topology, the properties of the solid material from which it was made, and its relative density (mass of the cellular material divided by that of the solid material from which the cellular material is made) [1]. Researchers are trying to improve the mechanical properties of cellular solids by developing new topologies. In recent years, auxetic honeycomb structures with negative Poisson's ratio have attracted numerous attentions. For a linear 3D isotropic material, the Poisson's ratio is bounded to a range from -1 to +1/2 due to thermodynamic stability [2]. In contrast, for a 2D isotropic material, the range of Poisson's ratio is from -1 to +1 [3]. Indeed, honeycomb with regular hexagonal cells has a Poisson's ratio approaching +1 in plane [1]. For both 2D and 3D anisotropic materials, the Poisson's ratio ~~e~~ is unbounded [4a, 4, 5]. It has been shown that auxetic honeycombs exhibited improved mechanical properties over conventional honeycombs [6-12]. Cellular solids can exhibit negative Poisson's ratios if the cell walls have an inverted bow-tie shape [13, 14], and such a topology is regarded as a classical re-entrant topology. Negative Poisson's ratio behaviour has been observed experimentally in polymer gels near phase transitions [15, 16], in orthorhombic alloy in a set of planes [17], in ferroelastic ceramic [18] and InSn alloy [19] near phase transformations, and also in certain in-plane directions in designed 2D and 3D structures [20-29]. However, the stiffness of re-entrant honeycombs is lower than that of the traditional honeycomb counterparts because of the structural geometry [30], as a result, there are limited structural applications of re-entrant honeycombs where structural stiffness is of the top desire [31]. Lu et al. [32] proposed a new topology concept by adding a narrow straight rib into the unit cell of classical re-entrant structure to improve the structure stiffness. The narrow straight rib is placed in such a way to connect the two concave vertices of the classical re-entrant unit cell. However, too high a stiffness reduces the auxetic response of the new topology.

In the present study, two new 2D re-entrant topologies with enhanced auxetic responses are introduced. Their Poisson's ratios and energy absorption capacities are studied using FEM as a function of geometric parameters. The first topology (model 1) was constructed by adding two sinusoidal shaped ribs into the unit cell of classical re-entrant topology, while the second topology (model 2) was made by introducing extra vertical ribs to reinforce the sinusoidal shaped ribs. Simulation results show that model 1 and model 2 can reach a minimum value in Poisson's ratio of -1.12 and -0.58 with an appropriate geometric aspect ratio, respectively. Enhanced energy absorption capacities were observed in these modified re-entrant topologies compared with the classical re-entrant topology. Model 2 exhibited the highest energy absorption capacity with a highest plateau stress. While, the plateau stress of model 1 was about half that of model 2, and when the compression velocity is more than 20m/s, the plateau stress of model 1 became lower than that of the classical re-entrant topology. The topologies proposed here could provide new opportunities for lightweight sandwich panel and energy absorption applications.

2. Materials and methods

Two types of modified re-entrant topologies with negative Poisson's ratio are developed in the present study. The unit cell of model 1 topology, as shown in Fig. 1a, is constructed by adding two sinusoidal shaped ribs with a length of period T and a peak-to-peak amplitude of

h_1 into the unit cell of the classical re-entrant topology [33]. Its geometry is defined by its height, H_0, length, L_0, and the depth of concavity, l_1, which determines the degree of re-entrant structure and behaviour. We define $H_0=L_0$ in the present study. Periodic packing of the model 1 unit cell creates a 2D re-entrant cellular structure as shown in Fig. 1(b). The unit cell of model 2 topology was created by introducing two vertical ribs of height h_2 into the unit cell of model 1 topology to serve as a reinforcement for the sinusoidal shaped ribs. Model 2 topology unit cell and the corresponding structure are shown in Fig. 1(c) and 1(d), respectively. A parameter, $\alpha=(h_0-h_2)/H_0$, was defined to determine the level of buckling of the introduced sinusoidal ribs. It is noted here that we keep the relative density the same for different types of re-entrant lattice structures by varying the wall thickness of the truss members, while all the truss members have the same wall thickness for a specific type of re-entrant lattice structure.

It will be shown later that Model 1 re-entrant lattice structure gives rise to the strongest auxetic response when $\alpha = 0.25$. Further investigation was thereafter performed to study the auxetic response of model 1 lattice structure to a change in the length of the sinusoidal shaped ribs; a length of half period (T/2) and one and a half periods (3/2T) for the sinusoidal shaped ribs were selected (Fig. 1) for this extra study. The relative density of lattice structures with different lengths of sinusoidal shaped ribs was kept the same by changing the truss member wall thickness.

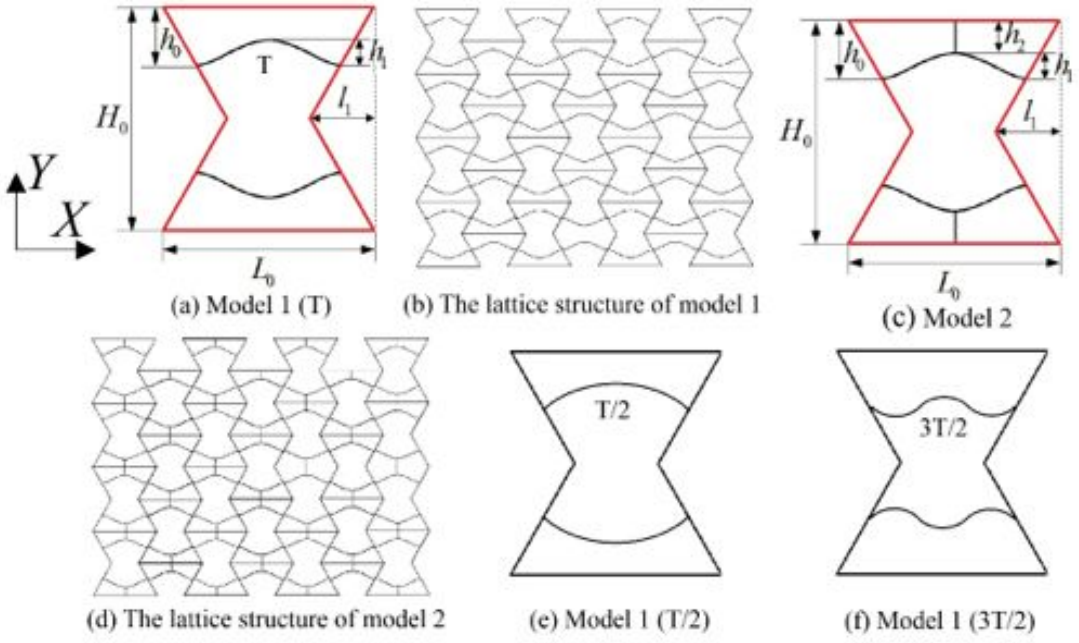

Figure 1. (a) Model 1 topology unit cell constructed by adding two one period (T) length sinusoidal shaped ribs into the classical re-entrant unit cell (the classical re-entrant unit cell is shown in red). Its corresponding lattice structure is shown in (b). (c) Model 2 topology unit cell constructed by adding reinforcement vertical ribs into model 1 topology unit cell. Its corresponding lattice structure is shown in (d). (e) Model 1 topology unit cell constructed by adding two half period (T/2) length sinusoidal shaped ribs into classical re-entrant unit cell. (f) Model 1 topology unit cell constructed by adding two one and a half periods (3T/2) length sinusoidal shaped ribs into classical re-entrant unit cell.

All the lattice structure models used for FEM simulations have a size of 276 x 200mm with 181 unit cells. Copper was selected as the parent material to provide ductile behaviour. It has a density of 8930 kg m^{-3}, Young's modulus of 117 GPa, and Poisson's ratio of 0.35. The lattice Poisson's ratio is independent of parent material properties but depends only on the geometry, yet the lattice collapse strength scales with the parent material strength. In this study, the lattice Poisson's ratio was investigated using ANSYS as a function of geometric parameter α. An α in the range from -0.25 to 0.25 was studied. A bilinear strain-hardening relationship was used to represent the true stress–strain relationship of the parent material, and the yield strength and tangent modulus were selected as 400MPa and 100MPa, respectively. The cell walls were meshed with Shell 163 elements (the number of elements depends on the edge length, and every edge had at least 5 elements). The Poisson's ratio was calculated from the elastic region of the stress strain diagrams obtained from the FE analysis. It is noted here that ANSYS does not take into account inertial effects and assumes time independent loading, and thus it studies the static mechanical responses. Therefore for dynamic studies, the following method was used.

ANSYS/LS-DYNA was used to analyze the energy absorption capacities of the proposed re-entrant structures at different compression velocities. ANAYA/LS-DYNA is specially designed to study dynamic response which takes into account inertia effects. The structures were compressed between two rigid platens with the bottom platen fixed, and the top platen moving at a constant velocity.

Results and discussion

3.1 Poisson's ratio

The relationship between the Poisson's ratio of the proposed re-entrant structures and the geometric parameter α ($-0.25 \leq \alpha \leq 0.25$) is shown in Fig. 2. It is noted that when α=0, the sinusoidal shaped ribs become straight ribs. It can be seen from Fig. 2 that the Poisson's ratio of model 1 topology first increased to a maximum value and then decreased with an increasing α, while the Poisson's ratio of model 2 topology increased monotonically with an increasing α. The Poisson's ratio of the two re-entrant topologies achieved minima of approximately -1.12 and -0.58 when $\alpha = 0.25$ and -0.25, respectively. The minimum Poisson's ratios of model 1 re-entrant lattice structures with half period (T/2) length and one and a half periods (3T/2) length sinusoidal shaped ribs are -1.17 and -1.32 when α=0.25 and -0.25, respectively. Compared with classical re-entrant lattice structure with the same geometric parameters, which has a Poisson's ratio of -1.424 (dot line as shown in Fig. 2), model 1 topologies exhibit comparable auextic responses.

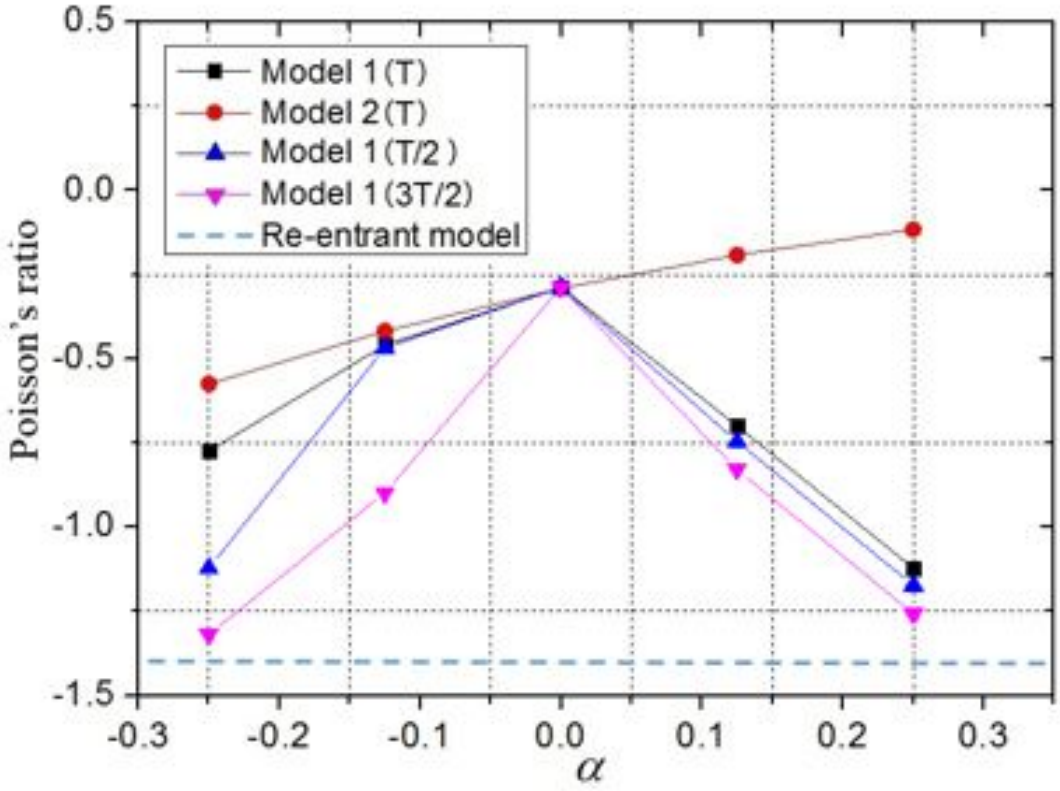

Figure 2. The relationship between the Poisson's ratio and α ($\alpha=(h_0-h_2)/H_0$) of modified re-entrant lattice structures. The Poisson's ratio of classical re-entrant lattice structure with the same geometric parameters is shown for comparison.

3.2 Energy absorption capacity

The energy absorption capacities of model 1 and 2 re-entrant lattice structures with one period length sinusoidal shaped ribs (Fig 1b and d) were analyzed at different compression velocities (from 2m/s to 60m/s), and their stress-strain diagrams are shown in Fig. 3. Responses of classical re-entrant lattice structure are also included for comparison. All three types of lattice structures have an identical relative density.

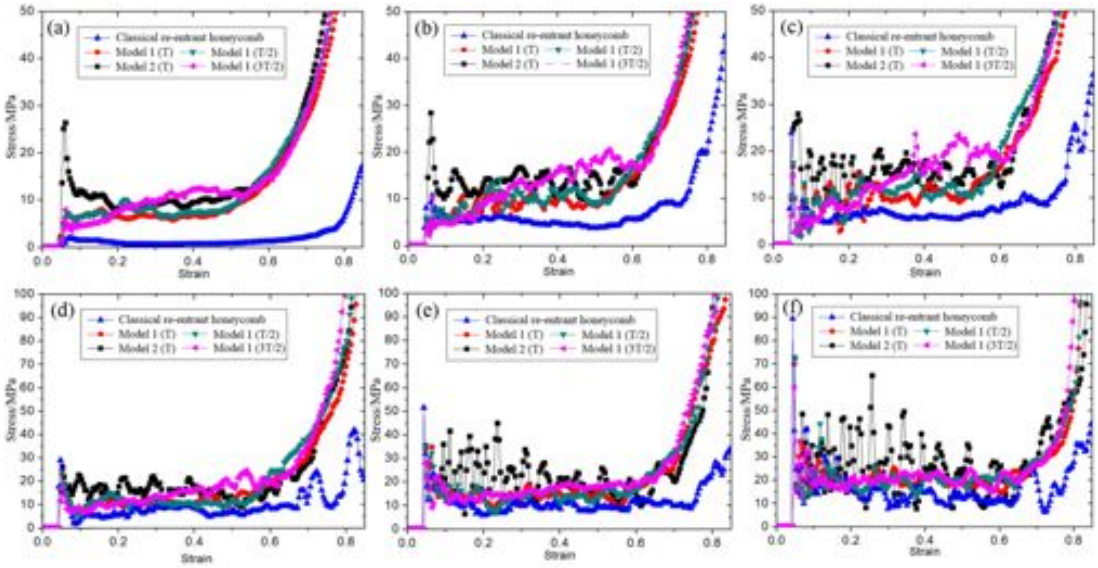

Fig. 3 The stress -strain diagrams of model 1 and model 2 re-entrant lattice structures with one period length sinusoidal shaped ribs and identical relative density at various compression velocities (a) v=2m/s; (b) v=5m/s; (c) v=10m/s; (d) v=20m/s; (e) v=40m/s; (f) v=60m/s. Classical re-entrant lattice structure responses are included for comparison.

The energy absorbed up to densification is commonly used to evaluate energy absorption capacity of cellular solids [6]. The energy absorption capacity per unit volume (W_v) of a lattice structure up to densification can be calculated via equation

$$W_v = \int_0^{\varepsilon_D} \sigma(\varepsilon) \mathrm{d}\varepsilon \tag{1}$$

where $\sigma(\varepsilon)$ is the plateau stress of the structure and ε_D is the densification strain which defines the strain beyond which the structure compacts and the stress rises steeply. The plateau is due to buckling of the ribs, or, if ribs are sufficiently thick, the plastic flow stress of the rib material [6].

Table 1 The energy absorption capacity per unit volume (W_v) of classical, model 1 and 2 re-entrant lattice structures with sinusoidal shaped ribs of various lengths of period at various compression velocities. All lattices have the same relative density.

Compression velocity(m/s)	W_v/MJm^{-3}				
	Classical	Model 1 (T)	Model 1 (T/2)	Model 1 (3T/2)	Model 2 (T)
2	0.6326	2.9780	2.5996	0.8792	7.4731
5	3.9573	4.1185	3.4660	1.5605	9.5618
10	5.5383	5.8794	5.8405	2.6926	9.7823
20	6.9000	7.6192	7.3567	5.3866	10.2608
40	9.8852	10.6909	11.5320	11.3644	14.4747
60	13.7338	15.5202	17.6848	16.9502	22.2510

Values of energy absorption per unit volume W_v of the classical, model 1 and model 2 re-entrant lattice structures at different compression velocities are summarized in Table 1. Results showed that the energy absorption capacity of all the models increased with an increasing compression velocity, and this trend is consistent with reports on auxetic structures [6, 12]. Model 2 topology gave rise to the highest energy absorption capacity while the classical re-entrant topology exhibited the lowest energy absorption capacity. The classical re-entrant topology exhibited a lower plateau stress compared with model 1 and 2 re-entrant topologies. Plateau stress of the five topologies increased with an increasing compression velocity, yet, that of the classical re-entrant topology exhibited a faster increasing rate compared with the other four topologies, and showed a comparable plateau stress as model 1 topology when the compression velocity is higher than 20m/s. Compared with the classical and model 1 re-entrant topologies, sharp undulations in flow stress were observed in the plateau region in model 2 topology. The energy absorption capacity of Model 1 topology with sinusoidal shaped ribs of various lengths of period was also studied. Results showed that, the energy absorption capacity of model 1 topology with one period (T) length sinusoidal shaped ribs was higher than those of model 1 topology with T/2 and 3T/2 lengths of ribs at a

compression velocity below 40m/s. When the compression velocity is higher than 40m/s, the energy absorption capacity of model 1 topology with T/2 and 3T/2 lengths of ribs become higher than that of topology with one period (T) length ribs.

Rate dependent energy absorption capacity of the lattice structures studied here is considered to be attributed to the inertia of the ribs. Energy absorption capacity of a lattice structure is highly dependent on its plateau stress level. Based on the sensitivity of plateau stress to the compression velocity, the applied compression velocity can be divided into three zones to distinguish ~~their~~ the relationships between velocity and behaviour: (1) quasi-static zone where plateau stress is insensitive to a change of compression velocity; (2) transition zone, and (3) dynamic zone where plateau stress is highly sensitive to a change in compression velocity. We found that the compression velocity no higher than 2m/s belongs to the quasi-static zone.

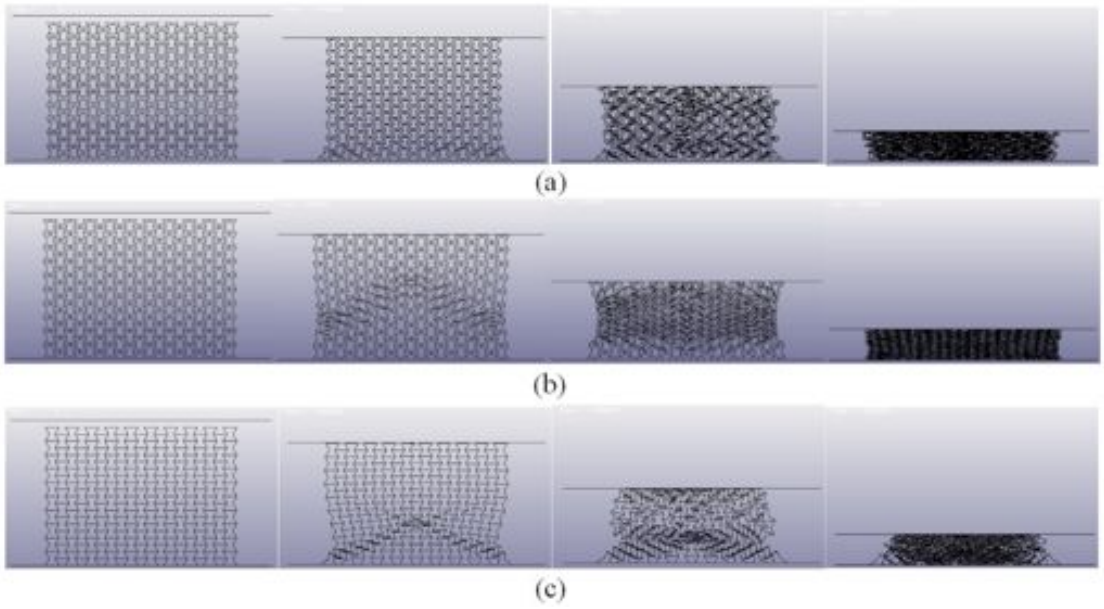

Fig. 4 Deformation mechanisms (a) model 1, (b) model 2 and (c) classical re-entrant lattice structures at a compression velocity v=2m/s.

The deformation mechanisms of the classical, model 1 and model 2 re-entrant topologies at a compression velocity of v=2m/s are shown in Fig.4. Localized "V"-shape crush bands were observed in the classical and model 2 re-entrant topologies, however, no such bands were observed in the model 1 topology. Collapse initiated near the fixed end, and propagated through toward the moving end.

4. Conclusions

Two new 2D re-entrant topologies with negative Poisson's ratio were introduced and their mechanical properties were studied using FEM as a function of geometric parameters. Simulation results show that model 1 and model 2 topologies can reach a minimum value in Poisson's ratio of -1.12 and -0.58, respectively, with an appropriate geometric aspect ratio. Results showed that the energy absorption capacity of all three models increased with an increasing compression velocity. Model 2 topology gave rise to the highest energy absorption capacity while the classical re-entrant topology exhibited the lowest energy absorption

capacity. The classical re-entrant topology exhibited a lower plateau stress compared with model 1 and 2 re-entrant topologies. Plateau stress of three topologies increased with an increasing compression velocity, yet, that of the classical re-entrant topology exhibited a faster increasing rate compared with the other two topologies, and showed comparable plateau stress as model 1 topology when the compression velocity is higher than 20m/s. Also, Localized "V"-shape crush bands were observed in the classical and model 2 re-entrant topologies, however, no such bands were observed in the model 1 topology. The new layout can be considered as a possible basis to design new concepts of auxetic structures with special functions.

Declaration of conflicting interests

Authors declare that no conflicting interests affected this research. Authors declare that no conflicting interests affected the objective presentation and description of results.

Acknowledgements

This work is supported by “The Fundamental Research Funds for the Central Universities (N150504006)”.

References

[1] Gibson L J, Ashby M F 1988 Cellular solids: structure & properties. Pergamon Press, Oxford

[2] Noll W, Antman S S, and Truesdell C 2004 The non-linear field theories of mechanics. Springer, Berlin

[3] Wojciechowski K W 2007 Remarks on "Poisson ratio beyond the limits of the elasticity theory", J Phys. Soc. JPN. 72(7) 1819-1820

[4a] Lempriere B M, 1968 Poisson's ratio in orthotropic materials AIAA Journal, 6, 2226-2227

[4] Ting T C T, Chen T 2005 Poisson's ratio for anisotropic elastic materials can have no bounds. Q. J. Mech. Appl. Math. 58, 73-82

[5] Grima J N, Caruanagauci R, Wojciechowski K W and Evans K E 2013 Smart hexagonal truss systems exhibiting negative compressibility through constrained angle stretching Smart Mater. Struct. 22(8) 084015

[6] Li D, Dong L, Yin J and Lakes R S 2016 Negative Poisson’s ratio in 2D Voronoi cellular solids by biaxial compression: a numerical study J. Mater. Sci. 51 7029-37

[7] Friis E A, Lakes R S and Park J B 1988 Negative Poisson’s ratio polymeric and metallic foams J. Mater. Sci. 23 4406-14

[8] Webber R S, Alderson K L and Evans K E 2008 A novel fabrication route for auxetic polyethylene: II. Mechanical properties Polym. Eng. Sci. 48 1351-8

[9] Lakes R S and Elms K E 1993 Indentability of conventional and negative Poisson’s ratio foams J. Compos. Mater. 27 1193-202

[10] Chan N and Evans K E 1998 Indentation resilience of conventional and auxetic foams J. Cell. Plast. 34 231-60

[11] Scarpa F and Tomlin P J 2000 On the transverse shear modulus of negative Poisson’s ratio honeycomb structures Fatigue Eng. Mater. Struct. 23 717-20

[12] Scarpa F, Ciffo L G and Yates J R 2004 Dynamic properties of high structural integrity

auxetic open cell foam Smart Mater. Struct. 13 49-56
[13] Gibson L J, Ashby M F, Schajer G S, Robertson C I 1982 The Mechanics of Two-Dimensional Cellular Materials Proc. Royal Society London, A382, 25-42.
[14] Kolpakov A G 1985 On the determination of the averaged moduli of elastic gridworks. Prikl Mat Mekh 59 969-977
[15] Hirotsu S 1991 Softening of bulk modulus and negative Poisson's ratio near the volume phase transition of polymer gels J. Chem. Phys. 94 3949-57
[16] Hirotsu S 1990 Elastic anomaly near the critical point of volume phase transition in polymer gels Macromolecules 23 903-5
[17] Rovati M 2003 On the negative Poisson's ratio of an orthorhombic alloy Scr. Mater. 48: 235-40
[18] Dong L, Stone D S and Lakes R S 2010 Softening of bulk modulus and negative Poisson ratio in barium titanate ceramic near the Curie point Phil. Mag. Lett. 90 23-33
[19] Li D, Jaglinski T M, Stone D S and Lakes R S 2012 Temperature insensitive negative Poisson's ratios in isotropic alloys near a morphotropic phase boundary Appl. Phys. Lett. 101 251903
[20] Hu H, Silberschmidt V 2013 A composite material with Poisson's ratio tunable from positive to negative values: an experimental and numerical study J Mater Sci, 48 8493-8500.
[21] Kaminakis N T, Stavroulakis G E 2012 Topology optimization for compliant mechanisms, using evolutionary-hybrid algorithms and application to the design of auxetic materialsComposites: Part B, 43 2655-68.
[22] Pozniak A A, Smardzewski J, Wojciechowski K W 2013 Computer simulations of auxetic foams in two dimensions Smart Mater Struct, 22 1-11.
[23] Li D, Dong L, Lakes R S 2016 A bi-material structure with Poisson's ratio tunable from positive to negative via temperature control. Materials Letters, 164 456-459.
[24] Baughman R H, Shacklette J M, Zakhidov A A, Stafstrom S 1998 Negative Poisson's ratios as a common feature of cubic metals Nature, 392 362-365.
[25] Grima J N and Evans K E, J. Mater. Sci. Lett. 2000 Auxetic behavior from rotating squares 19 1563-1565.
[26] Scarpa F, Blain S, Lew T, Perrott D, Ruzzene M, Yates J R 2007 Elastic buckling of hexagonal chiral cell honeycombs Compos A, 38, 280-289.
[27] Wojciechowski K W 1989 Two-dimensional isotropic system with a negative poisson ratio PHYS LETT A, 137, 60-64.
[28] Li D, Dong L, Lakes R S, 2013 The properties of copper foams with negative Poisson's ratio via resonant ultrasound spectroscopy Phys. Status Solidi B, 250, 1983-1987.
[29] Lakes R S 1987 Negative Poisson's Ratio Materials Science, 238 551.
[30] Prawoto Y. 2012 Seeing auxetic materials from the mechanics point of view: a structural review on the negative Poisson's ratio. Comput Mater Sci, 58 140-53
[31] Jones D. Handbook of viscoelastic vibration damping. New York: John Wiley and Sons; 2001.
[32] Zi-Xing Lu, Xiang Li, Zhen-Yu Yang, Fan Xie 2016 Novel structure with negative Poisson's ratio and enhanced Young's modulus. Composite Structures 138 243-252.
[33] Evans K E, Nkansah M A, Hutchinson I J, Rogers S C 1991 Molecular network design. Nature 353, 124-125